Journal of Alloys and Compounds 513 (2012) 524–529

Contents lists available at SciVerse ScienceDirect

Journal of Alloys and Compounds

journal homepage: www.elsevier.com/locate/jallcom

# Effects of $TiO_2$ crystal structure on the performance of $Li_4Ti_5O_{12}$ anode material

Feng Ning[a,b], Yan-Bing He[a], Baohua Li[a,*], Hongda Du[a], Dengyun Zhai[a,b], Feiyu Kang[a,b,**]

[a] Key Laboratory of Thermal Management Engineering and Materials, Graduate School at Shenzhen, Tsinghua University, Shenzhen 518055, China
[b] Laboratory of Advanced Materials, Department of Materials Science and Engineering, Tsinghua University, Beijing 100084, China

ARTICLE INFO

*Article history:*
Received 20 September 2011
Received in revised form 20 October 2011
Accepted 29 October 2011
Available online 9 November 2011

*Keywords:*
$TiO_2$ crystal structure
$Li_4Ti_5O_{12}$
Heat treatment
Electrochemical performance

ABSTRACT

$Li_4Ti_5O_{12}$ anode material is synthesized using $TiO_2$ with different crystal structure as titanium source by solid-state method. X-ray diffraction (XRD), scanning electron microscopy (SEM) and electrochemical test methods are applied to characterize the effects of $TiO_2$ crystal structure on the structure, morphology and electrochemical performance of $Li_4Ti_5O_{12}$. Results show that the reaction of $TiO_2$ with $Li_2CO_3$ is an exothermic behavior. The reactivity of $TiO_2$ with $Li_2CO_3$ gradually decreases and the particles size of $Li_4Ti_5O_{12}$ increases with the $TiO_2$ crystal structure changing from amorphous to rutile. The $TiO_2$ crystal structure has a slight influence on the reversibility of $Li_4Ti_5O_{12}$, while the specific capacities of $Li_4Ti_5O_{12}$ at different current densities decreases obviously with the $TiO_2$ crystal structure changing from amorphous to rutile and the sample using amorphous $TiO_2$ as titanium sources shows highest specific capacity. The capacity retentions of all $Li_4Ti_5O_{12}$ samples are above 97% after 50 cycles and these materials show good cycle performance. The $TiO_2$ crystal structure has not large effects on the cycling performance of $Li_4Ti_5O_{12}$ material.

© 2011 Elsevier B.V. All rights reserved.

## 1. Introduction

The fast development of electric vehicles has raised a strong demand for high-power and safety lithium ion power battery. However, at present, the anode material of graphite as the common anode material has high reactivity with electrolyte. Thus, the development of new anode materials with high safety and excellent performance are necessary and urgent for the development of electronic vehicle. Spinel $Li_4Ti_5O_{12}$ material has an excellent reversibility of Li-ion intercalation and de-intercalation with a theoretical capacity of 175 mAh $g^{-1}$, and also exhibits zero strain volume change during charge and discharge cycles with an excellent safety performance [1–3]. It also has a very flat voltage plateau at around 1.55 V (vs. $Li/Li^+$), which is higher than the reduction potential of most organic electrolytes [4–6]. Being much safer and more stable than carbon-based materials, $Li_4Ti_5O_{12}$ has been demonstrated as a good candidate of negative electrode material for long-life lithium-ion power batteries. Thus, the $Li_4Ti_5O_{12}$ material has become a research hotspot.

Currently the preparation methods of $Li_4Ti_5O_{12}$ materials mainly include solid-state and liquid-state methods. The solid-state method due to its simple synthesis, facile scale up and low cost has been used in many investigations for synthesis of $Li_4Ti_5O_{12}$ [7–13]. The factors, which influence the solid phase reaction, mainly include reaction temperature, reaction time and precursors. So far, there are many works to find the optimal reaction time and temperature for the synthesis of $Li_4Ti_5O_{12}$ materials, and it has been found that the general sintering temperature is between 800 and 1000 °C, and the holding time is mostly above 12 h [14,15,2,16,17]. It is well-known that the solid-state method usually uses the $TiO_2$ and $Li_2CO_3$/LiOH as the raw materials. Until now, the anatase $TiO_2$ is mainly used as the titanium source to synthesize the $Li_4Ti_5O_{12}$ [18,19]. In recent years, the amorphous $TiO_2$ and rutile $TiO_2$ also can be used to prepare the $Li_4Ti_5O_{12}$, which shows good electrochemical properties [18,20]. For instance, $Li_4Ti_5O_{12}$/C composite with long life can be synthesized using the amorphous $TiO_2$ [20]. The rutile $TiO_2$ after surface activation can be used to synthesize the $Li_4Ti_5O_{12}$, which shows the discharge capacity of ~175 mAh $g^{-1}$ at 1 C rate [18]. From above reports, it can be found that the preparation of $Li_4Ti_5O_{12}$ is only using one kind of $TiO_2$ as titanium source, and until now we do not know the effects of $TiO_2$ crystal structure on the performance of $Li_4Ti_5O_{12}$. In fact, the performance of $Li_4Ti_5O_{12}$ using different crystal structural $TiO_2$ as titanium source may be significantly different. Thus, it is very important to investigate the effects of $TiO_2$ crystal structure on the synthesis of $Li_4Ti_5O_{12}$ to further optimize the preparation conditions of $Li_4Ti_5O_{12}$.

In this work, we prepared the amorphous $TiO_2$ using microemulsion method as our previous work [20], and then amorphous $TiO_2$ was treated at different temperatures in air condition to obtain the

* Corresponding author. Tel.: +86 755 26036419; fax: +86 755 26036419.
** Corresponding author at: Key Laboratory of Thermal Management Engineering and Materials, Graduate School at Shenzhen, Tsinghua University, Shenzhen 518055, China. Tel.: +86 755 26036118; fax: +86 755 26036118.
*E-mail addresses:* libh@mail.sz.tsinghua.edu.cn (B. Li), fykang@mail.tsinghua.edu.cn (F. Kang).

0925-8388/$ – see front matter © 2011 Elsevier B.V. All rights reserved.
doi:10.1016/j.jallcom.2011.10.109

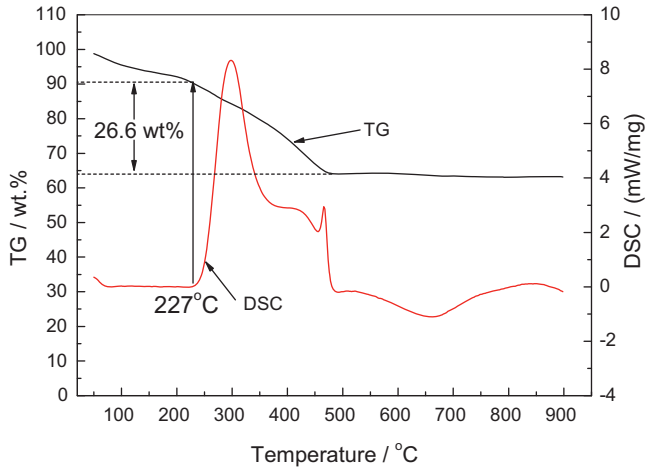


**Fig. 1.** TG-DSC curves of amorphous $TiO_2$.

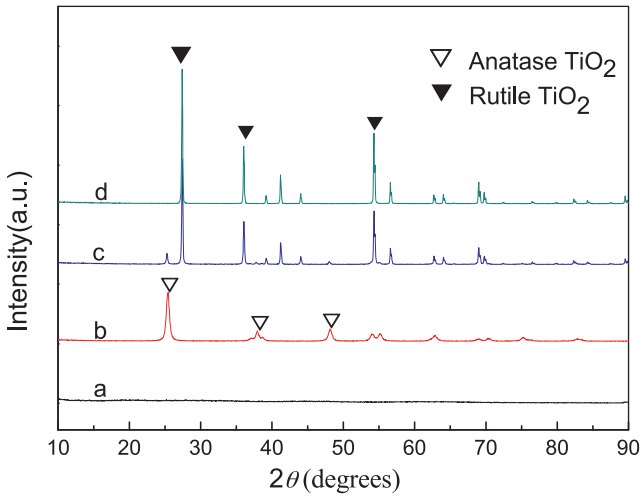


**Fig. 2.** XRD patterns of amorphous $TiO_2$ after treatment at different temperatures: (a) without heat treatment; (b) 450 °C; (c) 700 °C and (d) 900 °C.

anatase, hybrid phase containing both the anatase and rutile $TiO_2$, and rutile $TiO_2$. The $Li_4Ti_5O_{12}$ materials were prepared using above obtained $TiO_2$ and the effects of $TiO_2$ crystal structure on the performance of $Li_4Ti_5O_{12}$ anode material were investigated extensively.

## 2. Experimental

### 2.1. Preparation of $TiO_2$ nanoparticles

The saturated solution of cetyltrimethylammonium bromide (CTAB) was prepared with the deionized water under continuous stirring for 2 h. The butyl titanate ($Ti(OC_4H_9)_4$) was then added into the CTAB solution under ultrasound mixing. Then the stoichiometric ammonia was added under ultrasound mixing for 15 min and continuous stirring for 2 h. The resultant solution of amorphous $TiO_2$ was filtrated and dried to obtain the amorphous $TiO_2$ nanoparticles. Thermograyimetric (TG) and Differential Scanning Calorimetry (DSC) measurements for amorphous $TiO_2$ at air atmosphere were conducted with a heating rate of 10 °C $min^{-1}$ from 50 to 800 °C by using a NETZSCH STA449 C system. And then the prepared amorphous $TiO_2$ was treated under 450 °C, 700 °C, and 900 °C for 8 h at air condition, respectively, and the anatase, anatase and rutile hybrid phase, and rutile $TiO_2$ were obtained.

### 2.2. Preparation of $Li_4Ti_5O_{12}$ materials

$Li_4Ti_5O_{12}$ materials were synthesized by solid-state method using above obtained $TiO_2$ with the $Li_2CO_3$. The prepared $TiO_2$ and $Li_2CO_3$ were mixed at the Li:Ti molar ratio of 4.2:5. The precursors were ground for 6 h by a wet ball-milling in

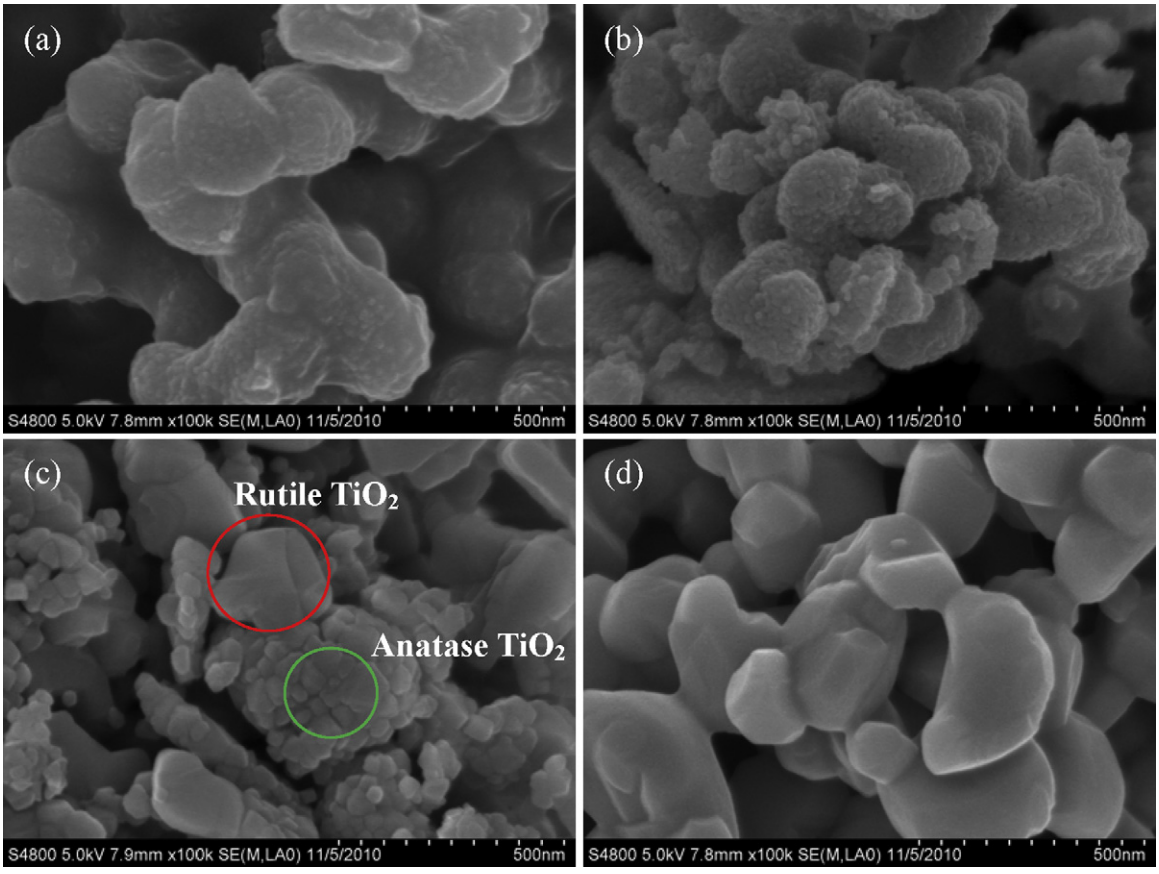


**Fig. 3.** SEM images of amorphous $TiO_2$ after heat treatment at different temperatures: (a) without heat treatment; (b) 450 °C; (c) 700 °C and (d) 900 °C.

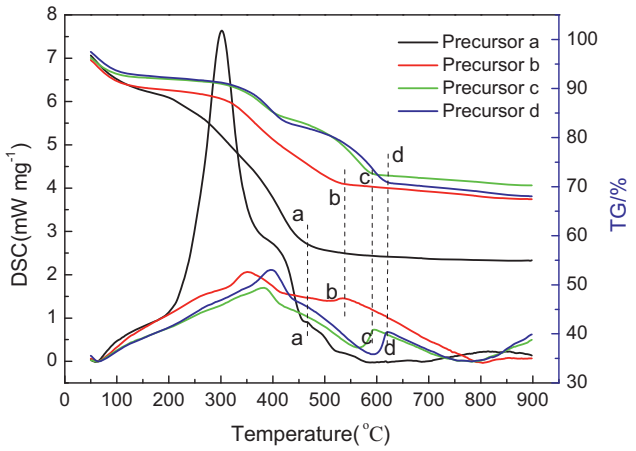


**Fig. 4.** TG-DSC curves of precursors of $Li_2CO_3$ and $TiO_2$ with different crystal structure: (a) amorphous $TiO_2$; (b) anatase $TiO_2$; (c) hybrid phase and (d) rutile $TiO_2$.

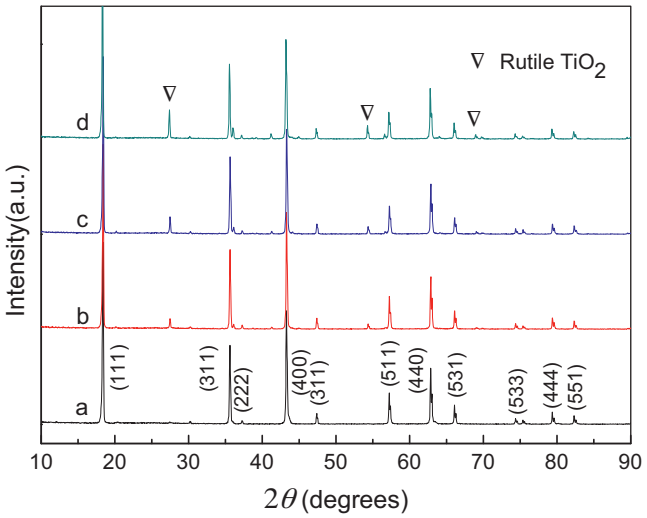


**Fig. 5.** XRD patterns of $Li_4Ti_5O_{12}$ synthesized using different crystal structural $TiO_2$: (a) amorphous $TiO_2$; (b) anatase $TiO_2$; (c) hybrid phase and (d) rutile $TiO_2$.

an acetone solution. The resultant stable gel was dried at 80 °C to form a mixed dry precursor. The dried powder precursor was then calcinated at 800 °C for 12 h in air atmosphere to obtain $Li_4Ti_5O_{12}$. TG-DSC measurements for precursors of prepared $TiO_2$ and $Li_2CO_3$ at air atmosphere were conducted with a heating rate of 10 °C min$^{-1}$ from 50 to 800 °C.

### 2.3. Structure and morphology characterization of prepared powders

X-ray diffraction (XRD) patterns of the prepared $TiO_2$ and $Li_4Ti_5O_{12}$ samples were obtained by a Rigaku D/max 2500/PC diffractometer using Cu Kα radiation in an angular range of 10–90° (2θ) with a 0.02° (2θ) step. The morphology of the prepared powders including $TiO_2$ and $Li_4Ti_5O_{12}$ was observed with an environment scanning electron microscope (FE-SEM, HITACH S4800).

### 2.4. Cell assembly and testing

2032 coin cells were assembled using the prepared $Li_4Ti_5O_{12}$ as cathode material, lithium foil as anode, and polypropylene as separator. The cathode consisted of 80 wt% $Li_4Ti_5O_{12}$, 10 wt% Super-P and 10 wt% poly(vinylidene fluoride) (PVDF). The electrolyte was 1 M $LiPF_6$ in a 1:1 mixture of ethylene carbonate and diethyl carbonate (1 M $LiPF_6$/EC + DEC). The cells were assembled in a glove box filled with high purity argon gas.

The electrochemical workstation (VMP3) was used to measure the cyclic voltammograms (CV) and the electrochemical impedance spectrum (EIS) of cells. EIS of the coin cells were measured at half state of charge using $Li_4Ti_5O_{12}$ as the working

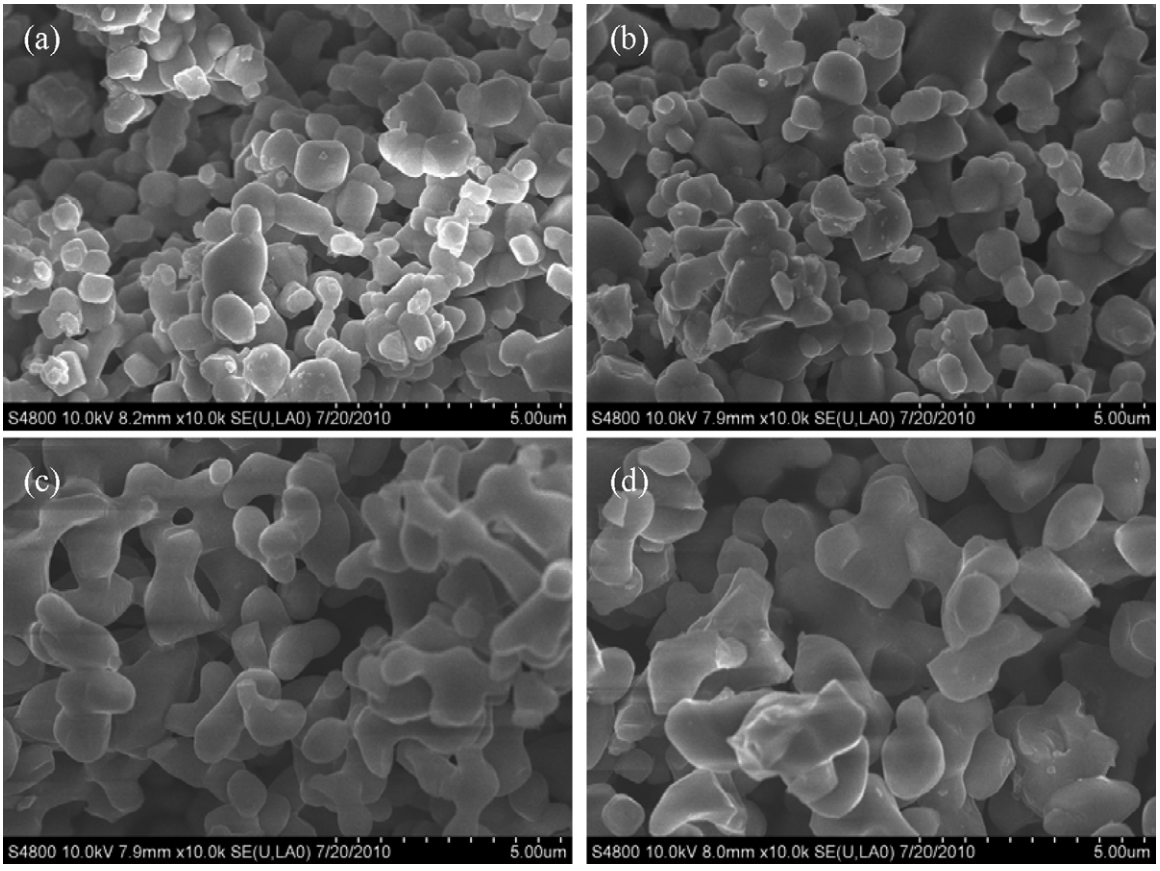


**Fig. 6.** SEM images of $Li_4Ti_5O_{12}$ synthesized using different crystal structural $TiO_2$: (a) amorphous $TiO_2$; (b) anatase $TiO_2$; (c) hybrid phase and (d) rutile $TiO_2$.

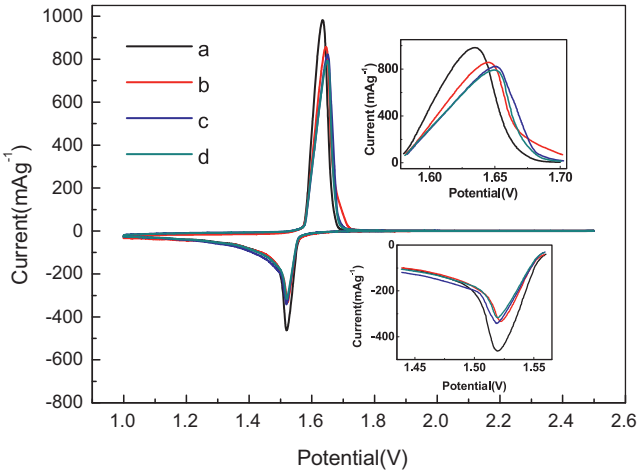


**Fig. 7.** CV of $Li_4Ti_5O_{12}$ synthesized using different crystal $TiO_2$: (a) amorphous $TiO_2$; (b) anatase $TiO_2$; (c) hybrid phase and (d) rutile $TiO_2$.

electrode and lithium as both the reference and counter electrodes. The impedance was measured by applying a 5 mV ac oscillation with the frequency ranging from 100 kHz to 0.01 Hz. The CV of coin cells were measured with $Li_4Ti_5O_{12}$ electrode as the working electrode, lithium foil as both the reference and counter electrodes. A scanning rate of 0.1 mV $s^{-1}$ was applied with a sweep voltage range of 2.5–1 V (vs. $Li/Li^+$). The cycling performance of $Li_4Ti_5O_{12}$ electrodes at current density of 17.5 mA $g^{-1}$ was examined by using a Land 2001A cell test system (Wuhan, China) at room temperature. The rate charge and discharge performance of $Li_4Ti_5O_{12}$ electrodes at current densities of 17.5, 87.5 and 175 mA $g^{-1}$ was also tested.

## 3. Results and discussion

### 3.1. TG-DSC measurement of amorphous $TiO_2$

Fig. 1 shows the TG-DSC curves of amorphous $TiO_2$ in air atmosphere. It can be observed that the DSC curve of sample has a sharp exothermic peak from 227 °C, which is corresponding with a main weight loss of 26.6 wt% in TG curve from 227 to 478 °C. This is due to decomposition and burning of CTAB and the content of CTAB in amorphous $TiO_2$ is 26.6 wt%. Thus, it can be obtained the content of carbon in amorphous $TiO_2$ is 16.6 wt%. Another sharp exothermic peak is found at about 450 °C, which may be attributed to the changing of $TiO_2$ crystal from amorphous to anatase. An endothermic peak is observed at around 660 °C, which may be due to the $TiO_2$ crystal changing from anatase to ruile.

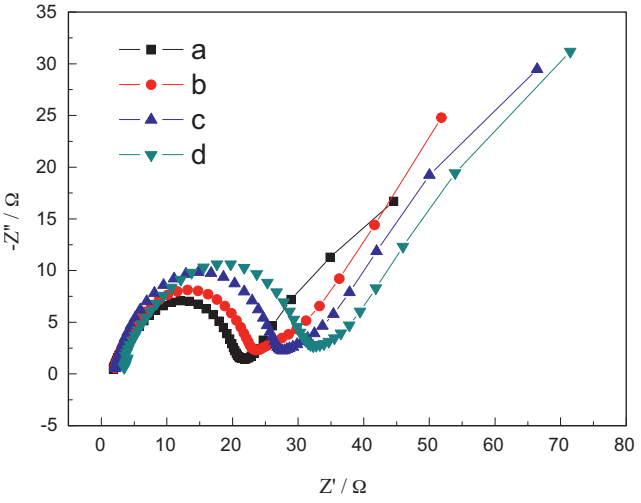


**Fig. 8.** EIS of $Li_4Ti_5O_{12}$ synthesized using different crystal structural $TiO_2$: (a) amorphous $TiO_2$; (b) anatase $TiO_2$; (c) hybrid phase and (d) rutile $TiO_2$.

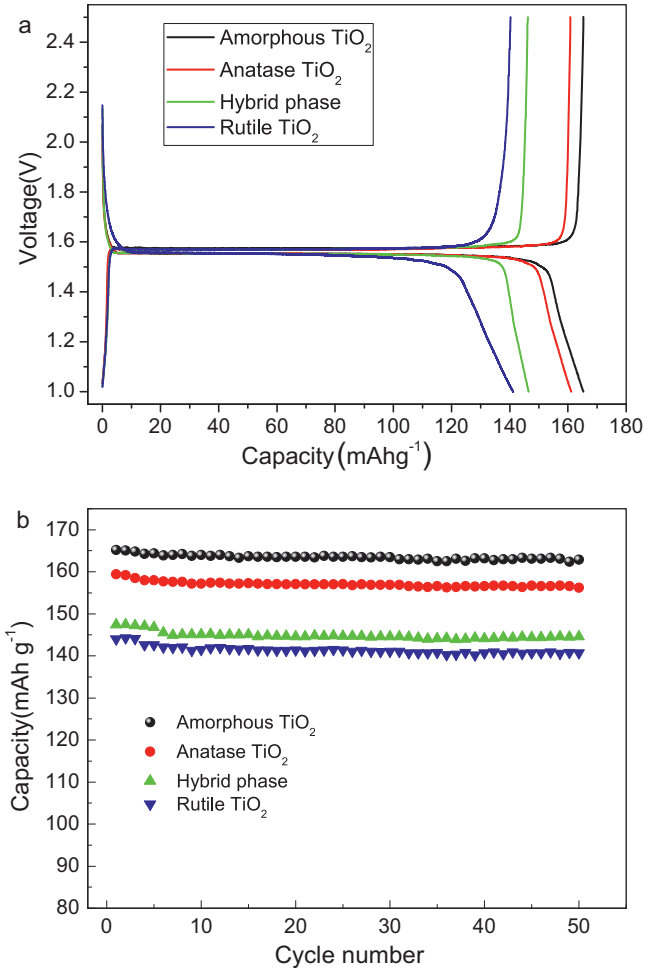


**Fig. 9.** Specific capacity (a) and cycling performance (b) of $Li_4Ti_5O_{12}$ synthesized using different $TiO_2$ with crystal structure of amorphous, anatase, hybrid phase and rutile.

### 3.2. Structure and morphology of $TiO_2$ nanoparticles

The XRD patterns of amorphous $TiO_2$ after heat treatment at different temperatures in air condition are shown in Fig. 2. It can be seen from Fig. 2a that the patterns of $TiO_2$ without heat treatment do not contain the peaks of the anatase and rutile phase. This suggests that the as-prepared $TiO_2$ without heat treatment is predominantly in amorphous phase. It can be observed from Fig. 2b and d that the patterns of $TiO_2$ after treatment at 450 °C and 900 °C is in good agreement with JCPDS file of anatase $TiO_2$ (card no. 21-1272) and rutile $TiO_2$ (card no. 21-1276), which suggests the formation of pure anatase and ruile $TiO_2$. Fig. 2c shows that the sample of $TiO_2$ consists of mixed anatase and rutile $TiO_2$ after the amorphous $TiO_2$ was treated under 700 °C for 8 h. Therefore, it can be concluded that the $TiO_2$ crystal treated at high temperature changes significantly along with the increase in treatment temperature, and the amorphous, anatase, anatase and rutile hybrid phase and rutile $TiO_2$ are obtained to use as the titanium source for synthesis of $Li_4Ti_5O_{12}$.

The SEM images of amorphous $TiO_2$ after heat treatment at different temperatures in air condition are shown in Fig. 3. As shown in Fig. 3a, the amorphous $TiO_2$ consists of spherical particles with average diameter of 200–300 nm, which are the agglomerates of much smaller primary particles with diameter of about 10–20 nm.

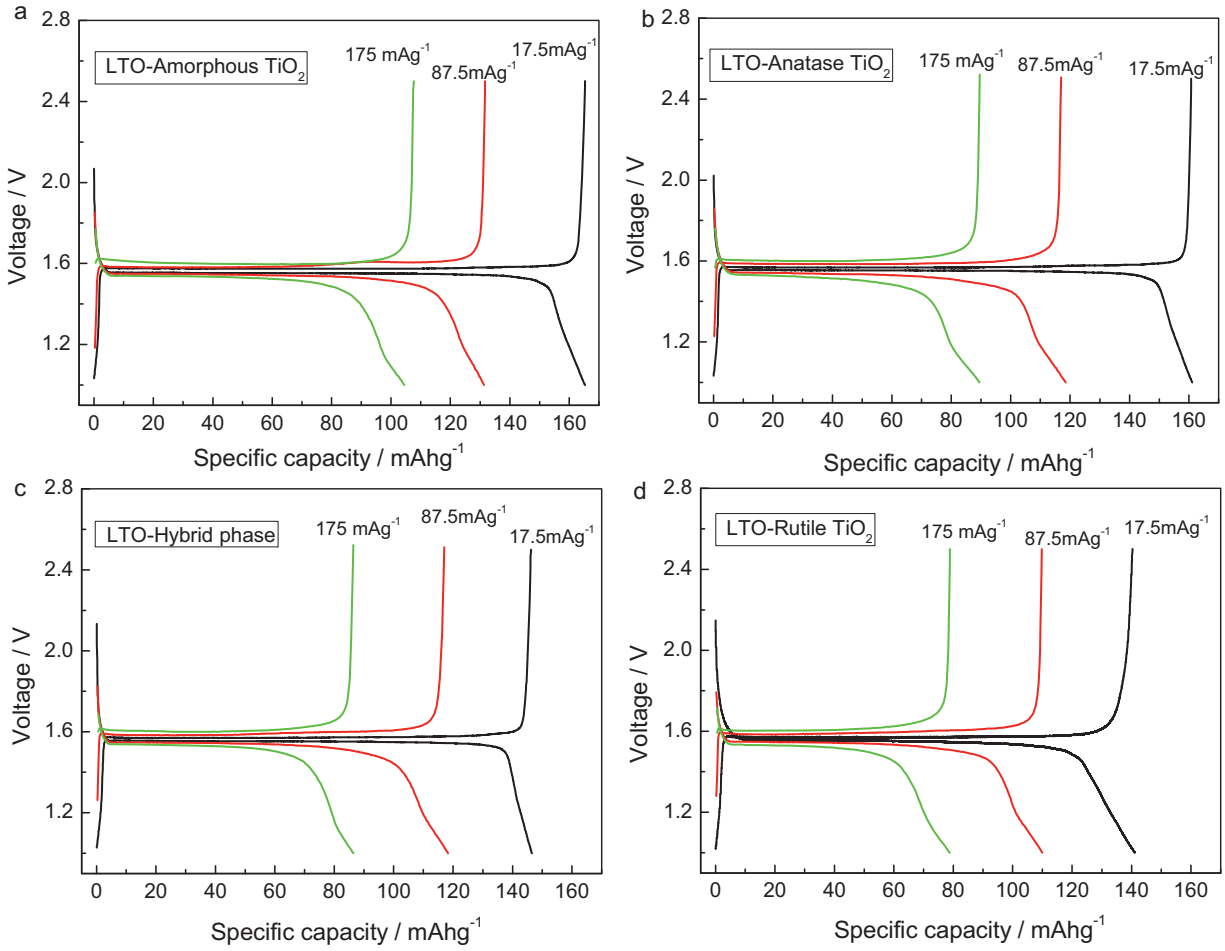


**Fig. 10.** Rate charge and discharge performance of $Li_4Ti_5O_{12}$ synthesized using different crystal structural $TiO_2$ at charge and discharge current densities of 17.5, 87.5 and 175 mA $g^{-1}$: (a) amorphous $TiO_2$; (b) anatase $TiO_2$; (c) hybrid phase and (d) rutile $TiO_2$.

The amorphous $TiO_2$ nanoparticles show highly ordered structure with well-defined secondary and primary particles. After heat treatment at 450 °C, it can be seen from Fig. 3b that the morphology $TiO_2$ does not change significantly and only the grain size of secondary particles has some decrease. This is due to the decomposition and burning of CTAB. Whereas, Fig. 3c shows that the morphology $TiO_2$ changes greatly after heat treatment at 700 °C. The sample consists of two type particles with obviously different grain size about 50 nm and 300 nm, respectively. When the amorphous $TiO_2$ is treated at 900 °C, Fig. 2d has shown that the sample is pure rutile $TiO_2$. From Fig. 3d, it can be obtained that the grain size of rutile $TiO_2$ is about 300–400 nm. Thus, it can be concluded that the small size particles in the sample after treatment at 700 °C is anatase $TiO_2$ and large size particles is rutile $TiO_2$.

### 3.3. Synthesis of $Li_4Ti_5O_{12}$ and morphology characterization

Fig. 4 shows the TG-DSC curves of precursors of $Li_2CO_3$ and $TiO_2$ with different crystal structure in air atmosphere. It can be observed from Fig. 4a that DSC curve of sample has a sharp exothermic peak at 300 °C, which corresponds with the main weight loss in TG curve from 200 °C to 350 °C. This is due to decomposition and burning of CTAB. Another exothermic peak is also found at 400 °C and a weight lose is observed on the TG curve at the temperatures ranging from 350 to 450 °C. This may be attributed to the loss of crystal water in the amorphous $TiO_2$ and decomposition of $Li_2CO_3$, and these two processes occur simultaneously. However, for the samples b, c and d, TG curves present that there is no further weight loss starting from temperatures of 540 °C, 600 °C and 630 °C, and an exothermic behavior can be observed on the DSC curves. This suggests that the decomposition reactions of $Li_2CO_3$ end and the reaction of $TiO_2$ with $Li_2O$ as the decomposition product is starting and this reaction is an exothermic reaction. Therefore, it can be found that the reactivity of $TiO_2$ with $Li_2CO_3$ gradually decreases with the $TiO_2$ crystal structure changing from amorphous to rutile, and the synthesis reaction of $Li_4Ti_5O_{12}$ becomes difficulty.

Fig. 5 shows the XRD patterns of $Li_4Ti_5O_{12}$ synthesized using $TiO_2$ with different crystal structure. It can be seen that the patterns of sample using the amorphous $TiO_2$ is in good agreement with JCPDS file (card no. 49-0207), confirming the formation of pure spinel $Li_4Ti_5O_{12}$ (Fig. 5a). While obviously impurity phase peaks of rutile $TiO_2$ can be observed in the Fig. 5b–d, and the peaks become stronger with $TiO_2$ crystal structure changing from the amorphous to rutile, which suggests an increase in the content of rutile $TiO_2$ in the $Li_4Ti_5O_{12}$. Therefore, it can be obtained that the reactivity of $TiO_2$ with $Li_2CO_3$ decreases significantly as the $TiO_2$ crystal structure changes from anatase to rutile. This result is corresponding with that of Fig. 4.

As shown in Fig. 6, the morphology of $Li_4Ti_5O_{12}$ synthesized using different crystal structure $TiO_2$ also change significantly. With the $TiO_2$ crystal changing from anatase to rutile, it can be seen that the particle size of $Li_4Ti_5O_{12}$ increases obviously and the adhesion between particles is more serious. This behavior is in good agreement with raw material of $TiO_2$ obtained at different temperatures treatment to amorphous $TiO_2$. Thus, the morphology, particle size and crystal structure of $TiO_2$ are very important for the synthesis of

$Li_4Ti_5O_{12}$ by solid-state method, which has a significant effect on the morphology and particle size of $Li_4Ti_5O_{12}$.

### 3.4. CV and EIS characterization of $Li_4Ti_5O_{12}$

Fig. 7 shows the CV of $Li_4Ti_5O_{12}$ synthesized using different crystal $TiO_2$. It can be seen that the cathodic peaks occur at 1.62, 1.64, 1.65 and 1.65 V for the $Li_4Ti_5O_{12}$ sample a, b, c and d, respectively, while the corresponding anodic peaks are all at around 1.52 V. The sample a using amorphous $TiO_2$ has a slightly higher lithiation potential and lower delithiation potential than those of other samples. And all samples show excellent reversibility. The EIS results of $Li_4Ti_5O_{12}$/Li half cells after three cycles are plotted in Fig. 8. All cells were cycled 3 times before the EIS measurement to ensure the complete formation of $Li_4Ti_5O_{12}$ electrode. It can be seen that all EIS patterns are composed of one depressed semicircle at high to middle frequency and a slope line at low frequency. The intersection of the slope line with real axis refers to a bulk resistance ($R_b$), which reflects the electronic and ionic resistance of two electrodes and electrolyte/separator. The depressed semicircle at high to medium frequency corresponds to the charge transfer resistance ($R_{ct}$) and its related double-layer capacitance ($C_{dl}$). The slopping line at low frequency represents the Warburg impedance, which is associated with lithium-ion diffusion in the $Li_4Ti_5O_{12}$ particles. It can be seen that the $R_b$ of $Li_4Ti_5O_{12}$ increases slightly when the $TiO_2$ crystal structure changes from anatase to rutile type, while the $R_{ct}$ increases significantly. The high $R_{ct}$ of $Li_4Ti_5O_{12}$ may be attributed to the larger particle size of $Li_4Ti_5O_{12}$, which is resulted from the lower reaction activities of rutile $TiO_2$ with $Li_2CO_3$.

### 3.5. Charge/discharge and cycling performance of $Li_4Ti_5O_{12}$

Fig. 9 shows the specific capacity and cycling performance of $Li_4Ti_5O_{12}$ synthesized using $TiO_2$ with different crystal structure at current density of 17.5 mA $g^{-1}$. It can be seen from Fig. 9a that all samples shows excellent change and discharge platform at around 1.55 V and the specific capacities are 167, 161, 147 and 144 mAh $g^{-1}$ for the samples a–d, respectively. The specific capacity decreases with the $TiO_2$ crystal structure changing from amorphous to rutile, and the sample using amorphous $TiO_2$ shows highest specific capacity. Fig. 9b presents the cycling performance of $Li_4Ti_5O_{12}$ samples. It can be observed that the capacity retentions of all samples are above 97% after 50 cycles and these materials show good cycle performance. Thus, the $TiO_2$ crystal structure has not large effects on the cycling performance of $Li_4Ti_5O_{12}$ material.

The rate charge and discharge performance of $Li_4Ti_5O_{12}$ synthesized using different crystal structural $TiO_2$ at charge and discharge current densities of 17.5, 87.5 and 175 mA $g^{-1}$ was tested as shown in Fig. 10. It can be seen that the discharge specific capacities at discharge current density 175 mA $g^{-1}$ for the $Li_4Ti_5O_{12}$ samples a–d are 107.7, 89.5, 86.4 and 78.9 mAh $g^{-1}$, respectively. The rate performance of $Li_4Ti_5O_{12}$ deteriorates with the $TiO_2$ crystal structure changing from anatase to rutile type. Therefore, it can be obtained that the $TiO_2$ crystal has significant effects on the rate charge and discharge performance. This may be attributed to the larger size of $Li_4Ti_5O_{12}$ particles and increase of impurity phase of rutile $TiO_2$ when the $TiO_2$ crystal structure changes from anatase to rutile type.

## 4. Conclusions

$TiO_2$ as the titanium source for the synthesis of $Li_4Ti_5O_{12}$ is very significant for the structure, morphology and electrochemical performance of $Li_4Ti_5O_{12}$ synthesized by solid-state method. In this work, $TiO_2$ with different crystal structure are prepared and used as the titanium source to investigate the effects of $TiO_2$ crystal structure on the performance of $Li_4Ti_5O_{12}$ anode material. It has been found that the structure, morphology and electrochemical performance of $Li_4Ti_5O_{12}$ are influenced significantly by the $TiO_2$ crystal structure. With the $TiO_2$ crystal structure changing from amorphous to anatase, hybrid phase and rutile $TiO_2$, the content of rutile $TiO_2$ phase in the $Li_4Ti_5O_{12}$ increases and the particles size also becomes larger, which leads to the decrease in the specific capacities of corresponding $Li_4Ti_5O_{12}$ at different current densities. However, the charge and discharge reversibility and cycling performance of $Li_4Ti_5O_{12}$ almost does not change with the $TiO_2$ crystal structure. In this work, the $Li_4Ti_5O_{12}$ material using amorphous $TiO_2$ shows best electrochemical performance.

## Acknowledgements

This work was supported by China Postdoctoral Science Foundation (No. 20100470296), National Natural Science Foundation of China (No. 50802049 and No. 50632040), Shenzhen Technical Plan Project (No. JP200806230010A and No. SG200810150054A), Guangdong Province Innovation R&D Team Plan for Energy and Environmental Materials.

## References

[1] E. Ferg, R.J. Gummow, A.d. Kock, M.M. Thackeray, J. Electrochem. Soc. 141 (1994) L147.
[2] T. Ohzuku, A. Ueda, N. Yamamoto, J. Electrochem. Soc. 142 (1995) 1431.
[3] L. Aldon, P. Kubiak, M. Womes, J.C. Jumas, J. Olivier-Fourcade, J.L. Tirado, J.I. Corredor, C.P. Vicente, Chem. Mater. 16 (2004) 5721.
[4] S.S. Zhang, K. Xu, T.R. Jow, Electrochim. Acta 51 (2006) 1636.
[5] H. Schranzhofer, J. Bugajski, H.J. Santner, C. Korepp, K.-C. Möller, J.O. Besenhard, M. Winter, W. Sitte, J. Power Sources 153 (2006) 391.
[6] S.S. Zhang, K. Xu, T.R. Jow, J. Power Sources 130 (2004) 281.
[7] T. Yuan, K. Wang, R. Cai, R. Ran, Z.P. Shao, J. Alloy Compd. 477 (2009) 665.
[8] T.F. Yi, J. Shu, Y.R. Zhu, X.D. Zhu, R.S. Zhu, A.N. Zhou, J. Power Sources 195 (2010) 285.
[9] D. Capsoni, M. Bini, V. Massarotti, P. Mustarelli, G. Chiodelli, C.B. Azzoni, M.C. Mozzati, L. Linati, S. Ferrari, Chem. Mater. 20 (2008) 4291.
[10] J. Wolfenstine, J.L. Allen, J. Power Sources 180 (2008) 582.
[11] S. Huang, Z. Wen, B. Lin, J. Han, X. Xu, J. Alloy Compd. 457 (2008) 400.
[12] S.H. Huang, Z.Y. Wen, X.J. Zhu, Z.H. Gu, Electrochem. Commun. 6 (2004) 1093.
[13] J. Shu, J. Solid State Electrochem. 13 (2009) 1535.
[14] K.M. Colbow, J.R. Dahn, R.R. Haering, J. Power Sources 26 (1989) 397.
[15] E. Ferg, R.J. Gummow, A. Dekock, M.M. Thackeray, J. Electrochem. Soc. 141 (1994) L147.
[16] S. Takai, M. Kamata, S. Fujine, K. Yoneda, K. Kanda, T. Esaka, Solid State Ionics 123 (1999) 165.
[17] K. Zaghib, M. Simoneau, M. Armand, M. Gauthier, J. Power Sources 82 (1999) 300.
[18] T. Yuan, R. Cai, P. Gu, Z.P. Shao, J. Power Sources 195 (2010) 2883.
[19] D.H. Wang, D.W. Choi, Z.G. Yang, V.V. Viswanathan, Z.M. Nie, C.M. Wang, Y.J. Song, J.G. Zhang, J. Liu, Chem. Mater. 20 (2008) 3435.
[20] B. Li, F. Ning, Y.-B. He, H. Du, Q.-H. Yang, J. Ma, F. Kang, C.-T. Hsu, Int. J. Electrochem. Sci. 6 (2011) 3210.